Effects of higher-order energy bands and temperature on the bosonic Mott insulator in a periodically modulated lattice

A. S. Sajna
Solid State Theory Division, Faculty of Physics, Adam Mickiewicz University, ul. Umultowska 85, 61-614 Poznań, Poland
(Received 15 January 2016; published 6 October 2016)

We show that a certain class of higher-order excitations in ultracold atoms experiments can be described by straightforward extension of the standard strong coupling approach in the coherent state path integral formalism. It is achieved by theoretical analysis of energy absorption spectroscopy in the three-dimensional system of strongly correlated bosons described by the Bose-Hubbard model. In particular, for unit filling, an explicit form of the single-particle Mott insulator Green function at finite temperatures is derived which goes beyond the standard Hubbard bands description. Moreover, for relevant densities, we calculated the energy absorption rate and performed thermometry on rubidium atomic cloud gas by using previously obtained experimental data. Within the local density approximation, we explain that in such systems the nature of absorption spectrum depends significantly on local chemical potential: (a) the crossover region between lobes is characterized by different types of particle-hole excitations from neighboring Mott lobes and (b) origin of higher-order energy excitations changes from hole type to particle type for higher bosonic densities.

DOI: 10.1103/PhysRevA.94.043612

I. INTRODUCTION

To fully understand the experimental results in ultracold lattice bosons experiments [1–3], it is important to study the impact of thermal fluctuations on atomic gases. In particular, phase diagrams [2,4–7], bosonic coherence [5,8–10], thermometry [11,12], dynamics [13–19], and thermalization [20] are examples of current advanced areas of study which give new insight into thermodynamics of strongly correlated particles.

One of the effective tools which have been used in experimental and theoretical examination of bosonic dynamics is based on periodical lattice modulation [3,17,21]. In this process, gas at certain characteristic energy scales absorbs energy, which provides a possibility to study the intrinsic many-body phenomena. However, assuming that the system is described by the Bose-Hubbard model (BHM) Hamiltonian [22–24], we also know that realistic experiments are not performed exactly at zero temperature and some thermally generated excitations appear. In such a situation it is natural to ask about the effects of these excitations on interpretation of experimental data. Answering this question is especially difficult because of the inhomogeneities introduced by the trapping harmonic potential [1,3,25,26]. This causes additional hopping effects between Mott shells [27–30] which can compete with excitation from thermally occupied sites [14]. Consequently, careful analysis of thermal fluctuations in such a system is needed. So far, for homogeneous systems, temperature effects on the energy absorption spectroscopy have been studied for one-dimensional [14] and Bethe lattices [15] giving better understanding of the underlying physics. Therefore, as the next step, it seems reasonable to include inhomogeneity of the gas with the help of the local density approximation (LDA). This enables direct qualitative comparison with experimental data and permits thermometry. In particular, on the one hand we have chosen a higher-dimensional lattice for which quantum fluctuations are less pronounced, and on the other hand we have used a geometry of the lattice which is currently realized in experiments in order to make qualitative comparison with experimental data. Therefore, in this paper we study a three-dimensional system of strongly correlated bosons on the optical lattice and we perform thermometry by using temperature dependence of spectral peaks [14], resorting to experimental data from Stöferle *et al.* [3]. Consequently, this allows us to assess the importance of thermal excitations in this system where we focus on the bosonic Mott phase.

Moreover, in order to properly describe thermal fluctuation, we should go beyond the standard Hubbard band description, whose role is also important in the analysis of quantum fluctuations within the BHM in the strongly correlated regime [27–35]. Consequently, the formalism presented in this paper could be regarded as a natural extension of analytical methods extensively studied so far in the literature within a random-phase-approximation-like scheme; i.e., strong coupling expansion in a coherent state path integral [36,37], and the equation of motion for Green functions [5,38–40]. The idea of the method corresponds to the earlier one which was used to study thermal properties of fermions and bosons within the slave particle formalism [41–43] and it is interesting on its own right.

In the following sections, we first describe the model and method applied (Sec. II). Next, in Sec. III, we use this method in the analysis of energy absorption rate and show its implications in understanding current experimental data. At the end we give a summary of our work (Sec. IV).

II. MODEL AND METHOD

A. Effective action

We analyze a system of strongly correlated bosons within BHM which is described by the Hamiltonian

$$H = -\sum_{\langle ij\rangle} t_{ij}\hat{b}_i^\dagger \hat{b}_j + \frac{U}{2}\sum_i \hat{b}_i^\dagger \hat{b}_i^\dagger \hat{b}_i \hat{b}_i - \mu \sum_i \hat{b}_i^\dagger \hat{b}_i. \quad (1)$$

where the parameters t_{ij}, U, and μ correspond to hopping, on-site interaction, and chemical potential energy, respectively. The sum over $\langle ij\rangle$ in Eq. (1) goes over nearest-neighbor sites.

Using the coherent state path integral formalism, we can obtain the following form of partition function:

$$\mathcal{Z} = \int \mathcal{D}b^*\mathcal{D}b\, e^{-(S_0+S_1)/\hbar}, \tag{2}$$

$$S_0 = \sum_i \int d\tau \Big\{ b_i^*(\tau)\hbar\partial_\tau b_i(\tau) + \frac{U}{2} b_i^*(\tau)b_i^*(\tau)b_i(\tau)b_i(\tau) - \mu b_i^*(\tau)b_i(\tau) \Big\}, \tag{3}$$

$$S_1 = -\sum_{\langle ij\rangle} \int_0^{\hbar\beta} d\tau\, t_{ij} b_i^*(\tau)b_j(\tau), \tag{4}$$

where the integrals in Eqs. (3) and (4) are taken over imaginary time τ and β is an inverse of temperature, i.e., $1/k_BT$ (where k_B is the Boltzmann constant). Furthermore, the standard strong coupling expansion theory is applied to BHM, in which S_1 term is treated as a perturbation [44]. In particular, this approach introduces the $\psi_i(\tau)$ field through the Hubbard-Stratonovich transformation, and the effective action to the second order in the $\psi_i(\tau)$ field reads

$$\tilde{S}_{\text{eff}} = \int_0^{\hbar\beta} d\tau\, t_{ij}\psi_i^*(\tau)\psi_j(\tau) - \frac{1}{\hbar}\sum_{ijk}\int_0^{\hbar\beta} d\tau\, d\tau' t_{ji}t_{ik} \times \langle b_i^*(\tau)b_i(\tau')\rangle_0 \psi_i^*(\tau')\psi_i(\tau), \tag{5}$$

where $\langle\cdots\rangle_0$ denotes the statistical average over action S_0 (i.e., $\langle\cdots\rangle_0 = Z_0^{-1}\int \mathcal{D}b^*\mathcal{D}b\cdots e^{-S_0/\hbar}$ and $Z_0 = \int \mathcal{D}b^*\mathcal{D}b\, e^{-S_0/\hbar}$). Truncating the above effective action $\tilde{S}_{\text{eff}}$ at the second order is justified in the Mott insulator (MI) phase, and in this paper we restrict our considerations to this phase.

Next, performing the Fourier transform to Matsubara frequency ω_n and wave-vector $\mathbf{k}$ space, the following form of effective action for nearest-neighbor hopping $t_{ij} = J$ is obtained:

$$S_{\text{eff}} = -\hbar\sum_{\mathbf{k}n}\psi_{\mathbf{k}n}^*\left[G^{MI}(\mathbf{k},i\omega_n) - J_{\mathbf{k}}^{-1}\right]^{-1}\psi_{\mathbf{k}n} = \sum_{\mathbf{k}n}\psi_{\mathbf{k}n}^*\left[-J_{\mathbf{k}} + \frac{1}{\hbar}J_{\mathbf{k}}^2 G_0(i\omega_n)\right]\psi_{\mathbf{k}n}. \tag{6}$$

where

$$\frac{1}{\hbar}G_0(i\omega_n) = -\sum_{n_0=M}^{N-1}\frac{(n_0+1)(f_{n_0+1}-f_{n_0})}{i\hbar\omega_n - (E_{n_0+1}-E_{n_0})}, \tag{7}$$

$$f_m = \frac{e^{-\beta E_m}}{\sum_{n_0=M}^{N} e^{-\beta E_{n_0}}}. \tag{8}$$

$J_k = -2J(\cos k_x + \cos k_y + \cos k_z)$ is a simple cubic tight-binding dispersion, $E_{n_0} = -\mu n_0 + Un_0(n_0-1)/2$ is an on-site energy of BHM in the $J = 0$ limit in which n_0 is an average density within a given Mott lobe, and $M = 0$ and $N \to \infty$. It is important to notice that, besides the definition of the MI Green function $G^{MI}(\mathbf{k},i\omega_n)$, Eq. (6), we introduce $-J_{\mathbf{k}}^{-1}$ for convenience because, after applying the Hubbard-Stratonovich transformation, we want to express the MI Green function in terms of the original $b_i(\tau)$ field, which is exactly $G^{MI}(\mathbf{k},i\omega_n)$ [45].

Finally, the bosonic Mott insulator can be described in terms of the MI Green function $G^{MI}(\mathbf{k},i\omega_n)$ from Eq. (6). The most common approach to this problem is based on the three-state approximation (TSA) [39,40,46,47] in which sums in Eqs. (7) and (8) are evaluated within the three indices n_0-1, n_0, n_0+1. In particular, if the Mott lobe with n_0 is considered then $M = n_0 - 1$ and $N = n_0 + 1$ (e.g., for the first lobe one has $M = 0$ and $N = 2$). So far the $G^{MI}(\mathbf{k},i\omega_n)$ form in TSA and at zero temperature ($\beta \to \infty$) has been widely studied in literature [5,36,39,41,44,47,48] (see also Appendix A). The finite temperature properties of the MI phase in TSA within $G^{MI}(\mathbf{k},i\omega_n)$ have been analyzed by Gerbier [49]. It is also worth mentioning here that there are also other TSA-like methods which have been used to investigate finite temperature effects [5,39,41].

In the next subsection, II B, we extend TSA in order to describe higher-order excitations.

B. Mott insulator phase in the higher-state approximation (HSA)

One of the main purposes of this paper is to investigate a finite temperature properties of the MI phase, where the TSA method fails. This happens in the higher-temperature regime, in which atoms start to redistribute within higher U bands and the standard Hubbard band description could be improper to fully describe current experimental setups [3,15]. Therefore, in further consideration, we go beyond TSA by including higher U-band quasiparticle excitations at finite temperatures. Formally in HSA this means that for $n_0 = 1$ we take $M = 0$ and $N = 3$ and for higher lobes ($n_0 \geqslant 2$) we take $M = n_0 - 2$ and $N = n_0 + 2$ in Eqs. (6)–(8). However, in further consideration, we mainly focus on the $n_0 = 1$ and $n_0 = 2$ cases, because a number of numerical and experimental studies have been conducted for these densities (see, e.g., [1–3,17,21,50,51]). Moreover, it is also worth mentioning here that the corresponding HSA was applied in the slave-boson and -fermion formalism [41–43], but so far this approximation has not been used to analyze the data from energy absorption spectroscopy, which is the main aim of this paper.

Now we focus on the $n_0 = 1$ case in HSA. Beyond the holon and doublon excitations presented in the standard TSA (see also Appendix A), HSA additionally takes into account the particle distributions on the lattice with three bosons at a site, i.e., triplons. Formally, different occupation probabilities of holons, singlons, doublons, and triplons at a site are described by f_0, f_1, f_2, and f_3, respectively. Evaluating Eqs. (6), (7), and (8) for $M = 0$ and $N = 3$ we get the following MI Green function:

$$G^{MI}(\mathbf{k},i\omega_n) = \frac{L(\mathbf{k},i\hbar\omega)}{[i\hbar\omega - E_h(\mathbf{k})][i\hbar\omega - E_p(\mathbf{k})][i\hbar\omega - E_t(\mathbf{k})]}, \tag{9}$$

$$E_{p/h}(\mathbf{k}) = A_{\mathbf{k}} - B_{\mathbf{k}}\sin\left(\frac{\pi}{6} \mp \frac{1}{3}\arccos C_{\mathbf{k}}\right), \tag{10}$$

$$E_t(\mathbf{k}) = A_{\mathbf{k}} + B_{\mathbf{k}}\cos\left(\frac{1}{3}\arccos C_{\mathbf{k}}\right), \tag{11}$$

$$A_{\mathbf{k}} = \tfrac{1}{3}(J_{\mathbf{k}} + 3U - 3\mu - 4J_{\mathbf{k}}f_3), \tag{12}$$

$$B_{\mathbf{k}} = \tfrac{2}{3}\sqrt{3U^2+J_{\mathbf{k}}(1-4f_3)^2+3J_{\mathbf{k}}U(-1+2f_1+4f_2-2f_3)}, \tag{13}$$

$$C_{\mathbf{k}} = -\frac{J_{\mathbf{k}}\left[9J_{\mathbf{k}}U(-1+2f_1+4f_2-2f_3)(-1+4f_3)+2J_{\mathbf{k}}^2(-1+4f_3)^3+9U^2(-1+6f_1-6f_2+4f_3)\right]}{2\left[3U^2+J_{\mathbf{k}}^2(1-4f_3)^2+3J_{\mathbf{k}}^2U(-1+2f_1+4f_2-2f_3)\right]^{3/2}}, \tag{14}$$

$$\begin{aligned} L(\mathbf{k},i\hbar\omega) = {} & (U-\mu-i\hbar\omega)(2U-\mu-i\hbar\omega)f_0-(2U-\mu-i\hbar\omega)(U+\mu+i\hbar\omega)f_1 \\ & +(\mu+i\hbar\omega)[(U+\mu+i\hbar\omega)f_2+3(U-\mu-i\hbar\omega)f_3], \end{aligned} \tag{15}$$

where in order to simplify the equations we use the identity $f_0+f_1+f_2+f_3=1$.

In the case of $n_0 \geqslant 2$, in order to get the explicit form of $G^{MI}(\mathbf{k},i\omega_n)$ in HSA, we need to consider $M=n_0-2$ and $N=n_0+2$ in Eqs. (6), (7), and (8), where four poles in $G_0(i\omega_n)$ are present. Then, to find an analytic expression for quasiparticles excitations from $G^{MI}(\mathbf{k},i\omega_n)$ in HSA corresponds to solving a polynomial of fourth order in terms of $i\hbar\omega$, which is straightforward because this kind of polynomial has an analytic solution [52]. However, we do not give here these lengthy results; instead we find quasiparticle poles and weights numerically for $n_0=2$, which is sufficient to understand the main results of this paper (see Sec. III).

In the following we use MI Green function described in this section to study the dynamics of BHM, but first we compare our results to those of the standard TSA approach. In further analysis, for simplicity we set $\hbar=1$ and $k_B=1$.

III. RESULTS

A. Comparison of HSA and TSA

In this section, we shortly discuss the opportunities of using HSA in comparison to the well-known results obtained so far in literature [49].

In Fig. 1(a), we present a comparison between TSA [49] and HSA phase boundaries at finite temperatures (at $T=0$, TSA and HSA give the same results). We observe that behavior of the critical line at finite temperatures is the same in the vicinity of the tips of Mott lobes; however, in the region between the lobes, the TSA method unveils a discontinuity. This shows that the TSA description between lobes fails, which can be overcome in the HSA method by extending the Hilbert space at a site. To determine the phase boundary, we use a condition for divergence of the single-particle MI Green function $G^{MI}(\mathbf{k},i\omega_n)$ [Eq. (6)] in the static limit, i.e. $J_{\mathbf{0}}G_0(i\omega_n=0)-1=0$ [see also Sec. II B and Eq. (A1) for the definition of $G_0(i\omega_n)$ in HSA and TSA].

In Figs. 1(b) and 1(c), by using HSA, we plot quasiparticle excitations in the MI phase ($T/U=0.1$) for $n_0=1$ and $n_0=2$, respectively. The two energy levels closest to zero are (a) quasiparticle excitations $|1\rangle \to |2\rangle$ for $n_0=1$ and $|2\rangle \to |3\rangle$ for $n_0=2$, and (b) quasihole excitations $|1\rangle \to |0\rangle$ for $n_0=1$ and $|2\rangle \to |1\rangle$ for $n_0=2$. Moreover, we can notice the correspondence between standard TSA and HSA, i.e., $E_p(\mathbf{k})$ and $E_h(\mathbf{k})$ in HSA correspond to quasiparticle $E^+_{TSA}(\mathbf{k})$ ($|1\rangle \to |2\rangle$) and quasihole $E^-_{TSA}(\mathbf{k})$ ($|1\rangle \to |0\rangle$) excitations in TSA, respectively [for TSA, see also Eqs. (A2)–(A3)]. The remaining bands in Figs. 1(b) and 1(c) describe the excitations from already thermally activated defects; i.e., for the first Mott lobe ($n_0=1$) triplon excitations appear which are related to the highest energy band ($|2\rangle \to |3\rangle$) and for the second lobe ($n_0=2$) there appear excitations with zero ($|1\rangle \to |0\rangle$) and four bosons ($|3\rangle \to |4\rangle$) at sites related to the lowest and the highest energy bands, respectively. Generally, in HSA for lobes with $n_0>1$, beyond the standard quasihole and quasiparticle excitations there will be thermally activated states with n_0-1 and n_0+1 over the MI ground state, implying n_0-2 and n_0+2 excitation, respectively.

It is also worth adding here that although HSA as a mean-field-like method gives only qualitatively correct answers for the phase boundary [Fig. 1(a)] [5], it should describe well the deep Mott insulator regime in which correlation length is short (i.e., for U/J values far away from phase boundary on the Mott insulator side, as in the parameter regimes

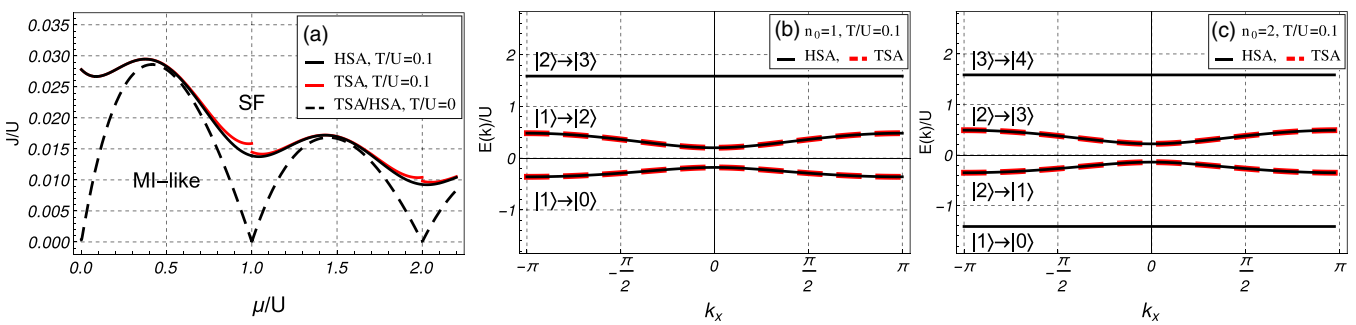

FIG. 1. (a) Phase diagram of the Bose-Hubbard model at $T/U=0.1$ for the three-state approximation (TSA) and higher-state approximation (HSA). For comparison, we plot the zero-temperature phase diagram at mean-field level (TSA/HSA). In the μ/U-J/U plane the red line corresponds to TSA at $T/U=0.1$, the black solid line to HSA at $T/U=0.1$, and the black dashed line to TSA/HSA at $T/U=0$. (b) and (c) correspond to the first and second lobes respectively, in which quasiparticle excitations in HSA and TSA are plotted. The remaining parameters are $J/U=0.025$, $\mu/U\approx 0.41$ for $n_0=1$ and $J/U=0.015$, $\mu/U\approx 1.41$ for $n_0=2$. In (b) and (c), we set also $k_y=k_z=0$.

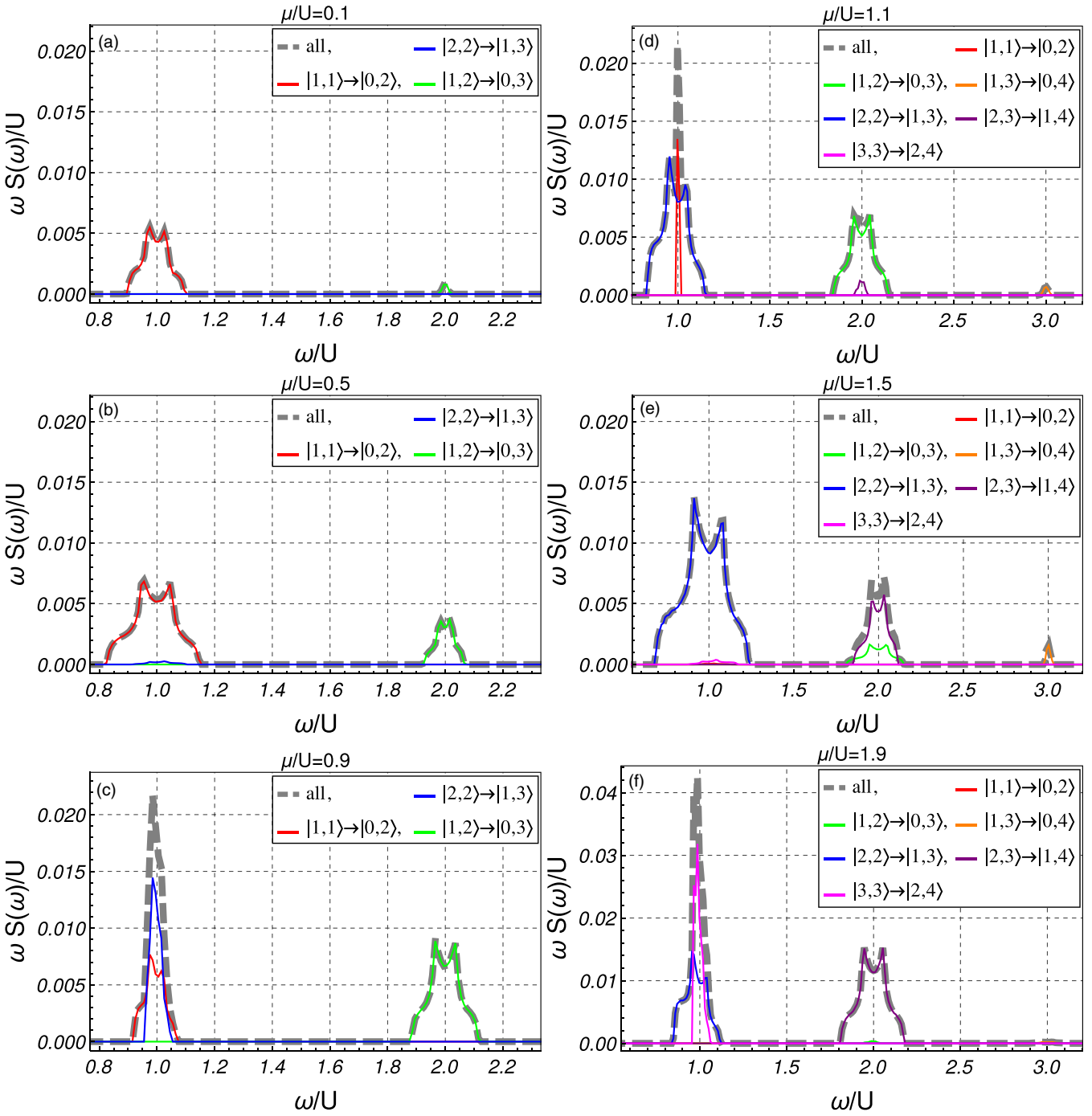

FIG. 2. HSA calculation of frequency ω/U dependent energy absorption rate in terms of $\omega S(\omega)/U$ for different values of chemical potential: (a) $\mu/U = 0.1$, (b) $\mu/U = 0.5$, (c) $\mu/U = 0.9$, (d) $\mu/U = 1.1$, (e) $\mu/U = 1.5$, (f) $\mu/U = 1.9$. Gray dashed line denotes the resultant effect of all transition types summed. Calculations are made at $T/U = 0.2$ with the interaction strength $U/J = 90$.

in Figs. 2 and 5). This is partially confirmed by previous studies at the zero-temperature limit in which HSA (and TSA also) quite well reproduce quantum Monte Carlo (QMC) results for large U/J values in one- and three-dimensional systems [35,53].

In the next subsection, we discuss the implication of the above energetic structure on the energy absorption rate in periodic lattice modulation experiments.

B. Spectroscopy by periodic lattice modulation

Lattice modulation technique [3,17,21] permits the study of higher-order excitations beyond the standard Hubbard bands, e.g., triplons which can appear over the MI ground state with unit density ($n_0 = 1$). In particular, this kind of spectroscopy tests energy absorption of the system at a given frequency ω by a lattice amplitude modulation periodic with time [19,54,55].

For anisotropy modulation of the lattice amplitude, e.g., in the x direction [3] and assuming the linear response regime [18,55], the system absorbs energy at a rate proportional to $\omega S(\omega)$ [47,55]. $S(\omega)$ is a kinetic energy autocorrelation [18,19,55] function which can be obtained from its Matsubara frequency representation,

$$\tilde{S}(i\omega) = \frac{1}{N}\int_0^\beta e^{i\omega\tau}\langle K(\tau)K(0)\rangle, \tag{16}$$

where the functional average is taken with the partition function from Eq. (2) (i.e., $\langle\cdots\rangle = Z^{-1}\int \mathcal{D}b^*\mathcal{D}b\cdots e^{-(S_0+S_1)/\hbar}$ and $Z = \int \mathcal{D}b^*\mathcal{D}b\, e^{-(S_0+S_1)/\hbar}$), $K(\tau) = J\sum_i b_i^*(\tau)b_{i\pm\delta x}(\tau)$ denotes the total kinetic energy in the x direction which includes the terms expressing hopping energy of atoms to nearest neighbors denoted by the vector $\pm\delta x$.

Knowing the explicit form of MI Green function from quadratic effective action, Eqs. (6)–(8), the correlation function in $\tilde{S}(i\omega)$ could be factorized and written in the form

$$\tilde{S}(i\omega) = \frac{4J^2}{N\beta}\sum_{\mathbf{k}n}\cos^2 k_x G^{MI}(\mathbf{k},i\omega_n)G^{MI}(\mathbf{k},i\omega_n + i\omega), \tag{17}$$

where $\omega_n = 2\pi n/\beta$ and we neglect terms which result later in a Dirac delta contribution at $\omega = 0$, because in this work we restrict our calculation to $\omega > 0$. Then, straightforward calculation can be performed to obtain $S(\omega)$, i.e., at first by evaluating the summation over Matsubara frequencies ω_n, taking the analytical continuation $i\omega \to \omega + i0^+$, and setting

$$S(\omega) = -\,\mathrm{Im}\,\tilde{S}(\omega + i0^+). \tag{18}$$

For the $n_0 = 1$ Mott lobe, using Eqs. (9)–(15), in HSA we get

$$\begin{aligned}\omega S(\omega) = \frac{\pi\omega}{N}\sum_{\mathbf{k}} 4J^2\cos^2 k_x \Bigg\{ &\frac{L(\mathbf{k},E_t(\mathbf{k}))L(\mathbf{k},E_p(\mathbf{k}))[f_B(E_t(\mathbf{k})) - f_B(E_p(\mathbf{k}))]}{(E_t(\mathbf{k}) - E_p(\mathbf{k}))^2(E_p(\mathbf{k}) - E_h(\mathbf{k}))(E_t(\mathbf{k}) - E_h(\mathbf{k}))}\delta(\omega - E_t(\mathbf{k}) + E_p(\mathbf{k})) \\ &+ \frac{L(\mathbf{k},E_t(\mathbf{k}))L(\mathbf{k},E_h(\mathbf{k}))[f_B(E_t(\mathbf{k})) - f_B(E_h(\mathbf{k})b)]}{(E_t(\mathbf{k}) - E_h(\mathbf{k}))^2(E_t(\mathbf{k}) - E_p(\mathbf{k}))(E_h(\mathbf{k}) - E_p(\mathbf{k}))}\delta(\omega - E_t(\mathbf{k}) + E_h(\mathbf{k})) \\ &+ \frac{L(\mathbf{k},E_p(\mathbf{k}))L(\mathbf{k},E_h(\mathbf{k}))[f_B(E_p(\mathbf{k})) - f_B(E_h(\mathbf{k}))]}{(E_p(\mathbf{k}) - E_h(\mathbf{k}))^2(E_p(\mathbf{k}) - E_t(\mathbf{k}))(E_h(\mathbf{k}) - E_t(\mathbf{k}))}\delta(\omega - E_p(\mathbf{k}) + E_h(\mathbf{k}))\Bigg\},\end{aligned} \tag{19}$$

where $f_B(x) = 1/[\exp(\beta x) - 1]$ is a Bose-Einstein distribution function and $\delta(x)$ denotes Dirac delta. Similar consideration in HSA can be made for the $n_0 = 2$ Mott lobe. However, because of the four types of excitation at finite temperatures, we treat this problem numerically (see also the discussion in Sec II B).

In Fig. 2, we present the energy absorption rate in terms of $\omega S(\omega)/U$ and characterize its behavior for different chemical potentials. Within the local density approximation (LDA), this analysis is directly related to the changes in chemical potential in the harmonic trap of ultracold atoms on optical lattices in which density decays as a function of distance from the trap center [56] (see also Secs. III C and III D in which LDA is discussed). Moreover, we choose a relatively high temperature $T/U = 0.2$ in order to better expose the role of thermal excitations. This temperature is also interesting on its own right because it is the melting temperature of the Mott insulator phase at finite temperatures [49]. However, before we discuss the results obtained at finite temperatures, we point out the zero-temperature limit of the energy absorption rate in Appendix B. This shows that relevant excitations in this limit start from the ground state, i.e., from single occupied states for the first lobe $|1,1\rangle \to |0,2\rangle$ [Fig. 4(a)] and double occupied states for the second lobe $|2,2\rangle \to |1,3\rangle$ [Fig. 4(b)] (see also Refs. [14,15]). At finite temperatures this picture is changed by thermal excitations over the MI ground state and becomes non-trivial within the HSA approach. This will be discussed in the following paragraphs.

As we expect for the finite temperature regime, the energy absorption around $\omega = U$ for the first lobe [$n_0 = 1$ and $\mu/U \in (0,1)$] and the second lobe [$n_0 = 2$ and $\mu/U \in (1,2)$] is dominated by particle-hole excitations $|1,1\rangle \to |0,2\rangle$ (red line) and $|2,2\rangle \to |1,3\rangle$ (blue line), respectively (Fig. 2). However, at finite temperature in the crossover region between $n_0 = 1$ and $n_0 = 2$ lobes (i.e., around $\mu/U = 1$), there are also precursor peaks of particle-hole excitations from the second lobe in the first one [Fig. 2(c)], and vice versa [Fig. 2(d)]. This higher-order excitation appears due to thermal defects caused by thermal fluctuations and gradual changes the U peak behavior. A similar situation starts to appear for $\mu/U = 1.9$ when we start to approach the third lobe ($n_0 = 3$). It is seen as a $|3,3\rangle \to |2,4\rangle$ precursor peak caused by thermally activated excitations [Fig. 2(f)]. We suppose that similar behavior will be observed for higher lobes. Therefore, this shows that finite-temperature effects extend particle-hole-like excitations beyond the area of the corresponding zero temperature Mott lobe. Consequently, the crossover region between lobes is characterized by different types of particle-hole excitations from neighboring Mott lobes [see Figs. 2(c), 2(d), and 2(f)].

If we consider energy absorption around $\omega = 2U$, its behavior for $n_0 = 1$ and $n_0 = 2$ differs. For the first lobe, a $2U$ peak emerges for higher chemical potential and is related to the increasing number of thermally activated doublons which cause triplon excitations $|1,2\rangle \to |0,3\rangle$ [Figs. 2(a)–2(c)]. Moreover, it is also the dominant mechanism of the $2U$ peak for the second lobe for lower chemical potential $\mu/U = 1.1$ [Figs. 2(d)]. Remarkably, if we increase μ/U further for the second lobe, the $2U$ peak gradually change its origin from hole-type defects $|1,2\rangle \to |0,3\rangle$ to particle-type ones $|2,3\rangle \to |1,4\rangle$, with intermediate behavior around $\mu/U = 1.5$. In particular, this result extend the recent work of bosonic dynamical mean-field theory (BDMFT) calculations

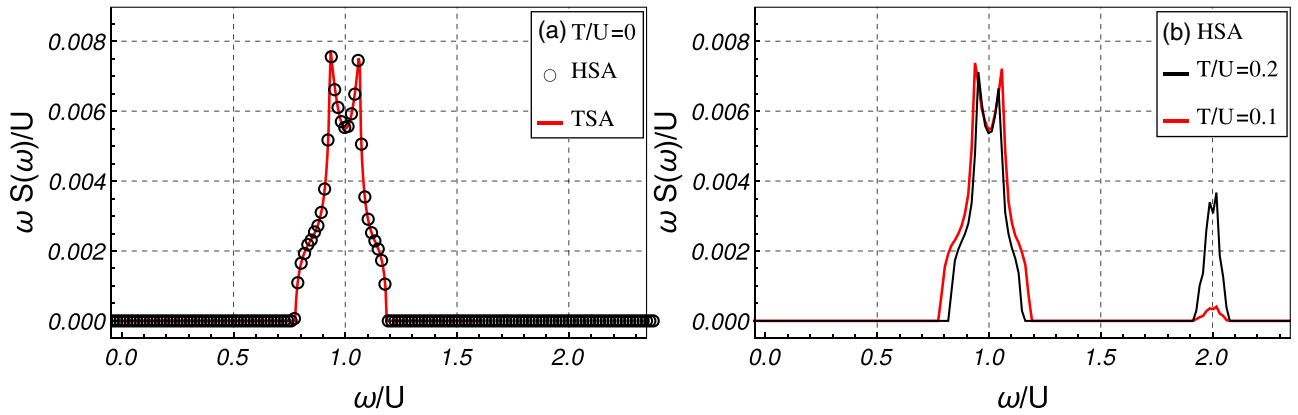

FIG. 3. $\omega S(\omega)$ in U units versus frequency ω/U for $\mu/U = 0.5$ where $n_0 = 1$. (a) Present HSA (black circles) and TSA (red line) results in the zero-temperature limit. In (b) the data points from HSA are plotted for $T/U = 0.1$ (red line) and $T/U = 0.2$ (black line).

[15] beyond half-integer values of μ/U, in which thermally activated side bands were also considered.

It is also worth pointing out that there is also a relatively small contribution to the energy absorption rate around $\omega = 3U$ for the second lobe caused by the $|1,3\rangle \rightarrow |0,4\rangle$ transition; see Figs. 2(d) and 2(e). This transition appears due to the presence of triplon and singlon thermal defects over the doubly occupied mean-field-like ground state of the second lobe.

Moreover, the occurrence of thermal defects depends naturally on temperature, and as an example in Fig. 3(b) we show that, for the first lobe, the $2U$ peak increases with higher temperature. This shows that more triplons are excited over the MI ground state as expected [see also Figs. 3(a)–3(c)]. However, in the limit $T \rightarrow 0$ double and triple excited states are suppressed due to the mean-field-like character of thermal excitations, and we checked that TSA results are recovered in this limit [see Fig. 3(a)]. From a technical point of view, this happens because the occupation probabilities for doublons f_2 and triplons f_3 vanish when $T \rightarrow 0$, and mean-field-like MI ground state with one particle per site on average are recovered (the only nonzero value is $f_1 = 1$). The $\omega S(\omega)$ within TSA is calculated in Appendix C.

C. Comparison with experiment

We compare our results with the experimental data from investigation of Rb^{87} atoms presented in Ref. [3]. In particular, we focus on the three-dimensional lattice in which strongly correlated effects between bosons were tested by using the amplitude modulation technique. In order to compare our results with those data, the harmonic potential caused by the magnetic trap and the Gaussian profile of the laser beams must be taken into account [56]. This could be effectively done by using the local density approximation to the BHM Hamiltonian from Eq. (1). This approximation shifts the chemical potential depending on the lattice position: $\mu \rightarrow \mu_i$, i.e., $\mu_i \rightarrow \mu_0 - V_t(\mathbf{r}_i - \mathbf{r}_0)^2$ [56], where μ_0 is the chemical potential at the center of the trap, $\mathbf{r}_i$ is the three-dimensional vector pointing to a given lattice site i, $\mathbf{r}_0$ is the position of the center of the trap (further we set $\mathbf{r}_0 = 0$), and $V_t = M/2(\omega_m^2 + 8V_0/Mw^2)$. The quantity V_t is defined by the atomic mass M, the frequency ω_m of the magnetic trap, the lattice depth V_0, and the waist w of the lattice beams. Then the quantity $\omega S(\omega)$, which is proportional to the energy absorption rate, in LDA can be translated to $\omega S_{\text{trap}}(\omega)$ where

$$\omega S_{\text{trap}}(\omega) = \sum_{\mathbf{r}_i} \left\{ \rho(\mathbf{r}_i)[\omega S(\omega)]_{\mu=\mu_0 - V_t \mathbf{r}_i^2} \right\}. \tag{20}$$

In Eq. (20), μ_0 is fixed by the number of atoms in the atomic cloud, i.e., $N = \int d\mathbf{r}\, \rho[\mu_0 - V_t \mathbf{r}^2]$. We set $N = 1.5 \times 10^5$ [3], and for simplicity we calculated the average density of atoms $\rho[\mu]$ in the atomic limit (i.e., $J = 0$) which is well satisfied for $J/U \ll 1$. For the other parameters we take values similar to those used in the experiment from Ref. [3], namely we set $\omega_m = 2\pi \times 20$ Hz, $w = 120$ μm. We are also focused on the strongly correlated regime in which we compare our results with the experimental data from the deep three-dimensional optical lattice $V_0 = 16E_r$. E_r is a recoil energy defined as $E_r = h^2/2M\lambda$ where λ is the laser wavelength equal to 826 nm [3]. In order to calculate the hopping and interaction energy in the BHM Hamiltonian [Eq. (1)], we use $J = \frac{4}{\sqrt{\pi}} E_r (V_0/E_r)^{3/4} e^{-2\sqrt{V_0/E_r}}$ and $U = 4\sqrt{2\pi}\frac{a}{\lambda} E_r (V_0/E_r)^{3/4}$, respectively [57].

In Fig. 5, we compare the data calculated from HSA and the experimental data from Ref. [3] for lattice depth $V_0 = 16E_r$. In order to investigate the $2U$ peak behavior, we normalized in vertical and horizontal axes the U peak from HSA to the U peak from Ref. [3]. Moreover, to better compare both sets of data, we use the same sampling of ω/U energy as in the experiment which, besides LDA, additionally washes out the internal structure of peaks coming from the three-dimensional lattice geometry (see Fig. 3). We observe that the $2U$ peak in HSA appears at the same position as the $2U$ peak from the experimental data. To get the best comparison with experiment, we adjusted the temperature to $T/U = 0.11$, which confirms that

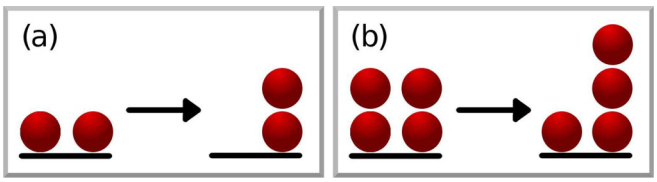

FIG. 4. Schematic explanation of (a) $|1,1\rangle \rightarrow |0,2\rangle$ and (b) $|2,2\rangle \rightarrow |1,3\rangle$ excitations.

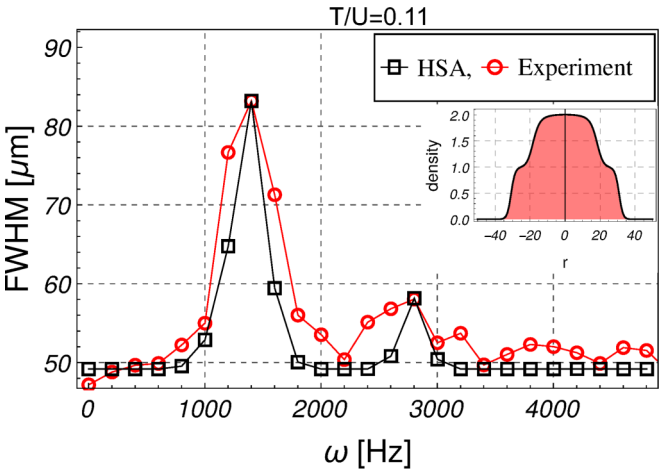

FIG. 5. The full width at half maximum (FWHM) as a measure of the introduced energy [3] compared with the frequency spectrum of $\omega S(\omega)/U$, which is proportional to the energy absorption rate. Black squares denote the data obtained within HSA and red circles denote the experimental data from Ref. [3]. To compare qualitatively the experimental data from Ref. [3] with HSA, we have normalized in vertical and horizontal axes the U peak from HSA to the U peak from Ref. [3], which enables analysis of the $2U$ peak behavior (see Secs. III C and III D). The inset shows the cross section of the average density distribution of the trapped gas. The simulation is made for $T/U = 0.11$.

the experiment was conducted in the regime in which bosonic Mott insulator properties still exist, i.e. $T/U < 0.2$ [49].

D. Discussion of HSA results

The thermometry presented in Sec. III C needs some more explanation. During the calculation, we neglected effects of nonlinear response and intershell hopping excitations. But as we explain below, those effects can at least increase the height ratio of $2U$ to U peak even further, causing the real temperature obtained from Fig. 5 to be lower than $T/U = 0.11$. This suggests that HSA gives the upper temperature limit, which is enough to confirm the quantum nature of the bosonic Mott insulator at finite temperature [49].

First, our linear response theory does not take into account nonlinear effects. They could be caused by relatively strong lattice amplitude modulation ($\approx$20% V_0) [3]. These effects can emerge as at least two-photon absorption events and as a saturation of absorbed energy. The first effect can give additional responses at around $U/2$ and $3U/2$ [29], so their contribution to U and $2U$ peaks can be neglected. Concerning the saturation effects, the relative height of U and higher peaks should grow faster than this from HSA [28,29], and then the $T/U = 0.11$ value of temperature would be an overestimation of a realistic temperature of the gas. However, no saturation effects were observed in Ref. [3], and therefore in the HSA analysis their effect could be neglected within U and $2U$ comparison as well.

Second, the situation concerning intershell hopping is more complex. Beyond higher-order excitations over the MI ground state at finite temperature, shown in Fig. 2, also intershell hopping between $n = 1$ and $n = 2$ could give an additional contribution to the vicinity of $2U$ absorption energy at which superfluid (SF) domains could exist [28–30] (here, for parameters from Fig. 5, only MI-like phases exist). However, in HSA, this contribution is neglected by LDA when a harmonic trap is taken into account. Although, if such SF domains exist, they could give an additional contribution to the $2U$ peak, confirming again that the $T/U = 0.11$ value is the upper boundary limit of realistic temperature. Consequently, HSA shows that a strongly correlated state of bosonic atoms in Ref. [3] was achieved.

Moreover, it is worth adding that for $T/U = 0.11$, the application of LDA can be justified due to relatively smoothly varying atomic density on the lattice even in the limit at which an SF phase does not exist [28]. The averaged atomic density of gas is shown in the inset of Fig. 5.

IV. SUMMARY

We have shown that a straightforward extension of the strong coupling theory, which includes higher-order energy bands (HSA), permits theoretical investigation of thermally activated excitations over strongly correlated bosonic ground states. This has allowed us to consider a three-dimensional system with realistic parameters from the experiment conducted by Stöferle *et al.* [3]. In particular, we could perform thermometry by analyzing the energy absorption spectrum and its dependence on temperature. Consequently, comparing theoretical and experimental data, we have given an upper bound for the temperature of the strongly correlated phase obtained in Ref. [3]. This confirms that a bosonic Mott insulator at finite temperatures was truly achieved (i.e., the estimated temperature satisfies $T/U < 0.2$ for which zero-temperature bosonic Mott insulator properties are still observed [49]).

Moreover, within the local density approximation, we have shown that in the Mott insulator phase at finite temperatures the nature of the absorption spectrum depends significantly on the local chemical potential. This analysis reveals that particle–hole-like excitations extend beyond the area of the corresponding zero temperature Mott lobe, and the origin of higher-order energy excitations changes from hole type to particle type for higher bosonic densities.

We can conclude that the method presented in this paper can be a relevant starting point for further investigation of finite-temperature properties of strongly correlated bosonic systems with different geometries. Moreover, it could be also interesting to compare obtained finite-temperature results with those from more sophisticated methods, such as quantum Monte Carlo (QMC) [58–60]. This is because the validity of the zero temperature limit of HSA (and TSA as well) has been partially confirmed by QMC for a deep Mott insulator regime [35,53], and further comparison of QMC and HSA at finite temperature would be also interesting. Summarizing, we believe that HSA as an analytical method should be an efficient approach to simulate the deep Mott insulator regime of real systems at finite temperatures.

ACKNOWLEDGMENTS

We would like to thank to M. Köhl for sharing experimental data presented in Fig. 5. We are also grateful to R. Micnas,

T. P. Polak. and P. Rożek for valuable discussions and as well as to R. Micnas and T. P. Polak for carefully reading of the manuscript. This work was partially supported by the National Science Centre, Poland, Project No. 2014/15/N/ST2/03459.

APPENDIX A: THREE-STATE APPROXIMATION (TSA)

In the main text, we have made a comparison of HSA to TSA, therefore for clarity we give here the TSA single-particle Green function. In particular, taking $M = n_0 - 1$ and $N = n_0 + 1$ in Eqs. (6)–(8), for a given n_0th lobe, we get $G^{MI}_{TSA}(\mathbf{k}, i\omega_n) = [\hbar G_0^{-1}(i\omega_n) - J_{\mathbf{k}}]^{-1}$, where

$$\frac{1}{\hbar}G_0(i\omega_n) = -\frac{(n_0+1)(f_{n_0+1} - f_{n_0})}{i\hbar\omega_n - (E_{n_0+1} - E_{n_0})} - \frac{n_0(f_{n_0} - f_{n_0-1})}{i\hbar\omega_n - (E_{n_0} - E_{n_0-1})} \tag{A1}$$

and quasi-particle excitations are

$$E^{\pm}_{TSA}(\mathbf{k}) = \frac{J_k}{2}[f_{n_0-1,n_0}n_0 + f_{n_0,n_0+1}(n_0+1)] - \mu + U\left(n_0 - \frac{1}{2}\right) \pm \frac{1}{2}\Delta(\mathbf{k}), \tag{A2}$$

$$\Delta(\mathbf{k}) = \left\{U^2 + 2J_kU[(n+1)f_{n_0,n_0+1} - n_0 f_{n_0-1,n_0}] + J_k^2[n_0 f_{n_0-1,n_0} + (n_0+1)f_{n_0,n_0+1}]^2\right\}^{1/2}, \tag{A3}$$

where for simplicity we have introduced the notation $f_{\alpha\beta} = f_\alpha - f_\beta$ (see also [49]). It is also worth mentioning that there are a number of other methods approximating f_α parameters [5,39,41]. In the limit of $T \to 0$, Eqs. (A2) and (A3) give a well-known RPA-like excitation spectrum [5,36,39,41,44,47,48], i.e., $E^{\pm}_{TSA}(\mathbf{k}) = J_{\mathbf{k}}/2 - \mu + U(n_0 - 1/2) \pm \Delta(\mathbf{k})/2$ and $\Delta(\mathbf{k}) = [U^2 + 2J_kU(2n+1) + J_{\mathbf{k}}^2]^{1/2}$.

For clarity, in particle notation, $E^{+}_{TSA}(\mathbf{k})$ corresponds to the $|n_0\rangle \to |n_0+1\rangle$ transition and $E^{-}_{TSA}(\mathbf{k})$ corresponds to the $|n_0\rangle \to |n_0-1\rangle$ transition; e.g., for $n_0 = 1$ these are doublon and holon excitations, respectively.

APPENDIX B: ENERGY ABSORPTION RATE IN HSA AT $T = 0$

In Fig. 6 we present $\omega S(\omega)/U$ calculation at zero temperature in HSA for different chemical potentials. As we can expect, the absorption of energy takes place only for the energy scale proportional to interaction energy U, which is caused by particle-hole excitations over the Mott insulator ground state; i.e., the $|1,1\rangle \to |0,2\rangle$ transition for the first lobe ($\mu/U = 0.7$) and the $|2,2\rangle \to |1,3\rangle$ transition for the second lobe ($\mu/U = 1.3$ and $\mu/U = 1.7$) (see also [14,15]). Moreover, as we expect for $T \to 0$ in HSA, the response of the system within a given Mott lobe does not depend on chemical potential μ/U, because of approaching the TSA limit [compare Figs. 6(b) and 6(c)] [37,47,61].

APPENDIX C: ENERGY ABSORPTION RATE IN TSA AT $T = 0$

The energy absorption rate is proportional to $\omega S(\omega)$ [47,55] and, in TSA at $T = 0$, $\omega S(\omega)$ is given by

$$\omega S(\omega) = \sum_{s=\{+,-\}} \frac{4\pi J n_0(1+n_0)}{\sqrt{4n_0(1+n_0)+\omega^2}}\rho(u^s(\omega)), \tag{C1}$$

$$u^{\pm}(\omega) = \frac{(2n_0+1)}{J}\left(1 \mp \sqrt{1 - \frac{1-\omega^2}{(2n_0+1)^2}}\right), \tag{C2}$$

where J and ω are given in U units and

$$\rho(v) = \Theta\left(1 - \left(\frac{u}{4}\right)^2\right)\Theta(4 - (v+u)^2) \times \int du \frac{\left(\frac{1}{2} + \left(\frac{u}{4}\right)^2\right)\mathcal{K}\left(\sqrt{1 - \left(\frac{u}{4}\right)^2}\right) - \mathcal{E}\left(\sqrt{1 - \left(\frac{u}{4}\right)^2}\right)}{\pi^3\sqrt{4 - (v+u)^2}} \tag{C3}$$

is a three-dimensional density of states with $\cos^2 k_x$ weight, i.e., $\rho(v) = (1/N)\sum_{\mathbf{k}} \cos^2(k_x)\delta(v + J_{\mathbf{k}}/J)$ with a step function Θ. Equation (C1) is obtained in analogy to Eq. (19) but using the TSA Green function $G^{MI}_{TSA}(\mathbf{k}, i\omega_n)$ from Appendix A. For the analogous calculation see Refs. [37].

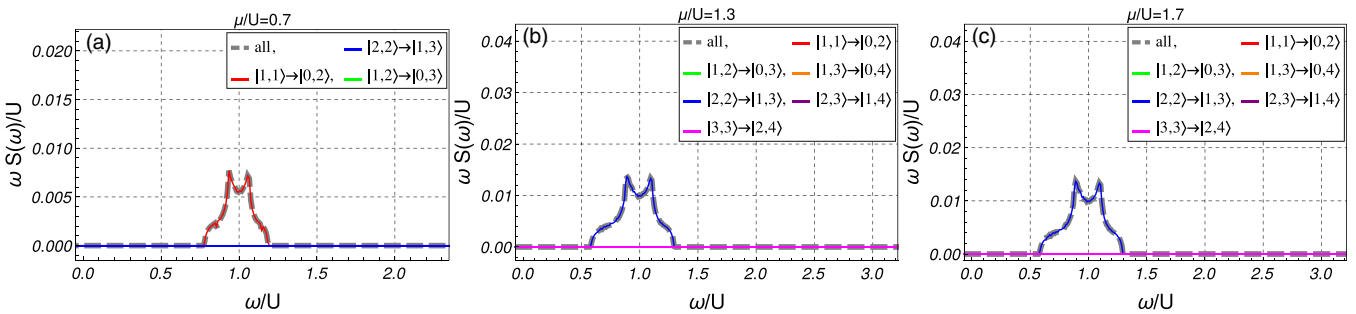

FIG. 6. HSA calculation of frequency ω/U dependent energy absorption rate in terms of $\omega S(\omega)/U$ for different values of chemical potential: (a) $\mu/U = 0.7$, (b) $\mu/U = 1.3$, (c) $\mu/U = 1.7$. Gray dashed lines denote the resultant effect of all transition types summed together. Calculations are made at $T/U = 0$ with interaction strength $U/J = 90$.

[1] M. Greiner, O. Mandel, T. Esslinger, T. W. Hänsch, and I. Bloch, Nature (London) **415**, 39 (2002).
[2] S. Trotzky, L. Pollet, F. Gerbier, U. Schnorrberger, I. Bloch, N. V. Prokof'ev, B. Svistunov, and M. Troyer, Nat. Phys. **6**, 998 (2010).
[3] T. Stöferle, H. Moritz, C. Schori, M. Köhl, and T. Esslinger, Phys. Rev. Lett. **92**, 130403 (2004).
[4] B. Capogrosso-Sansone, N. V. Prokof'ev, and B. V. Svistunov, Phys. Rev. B **75**, 134302 (2007).
[5] A. S. Sajna, T. P. Polak, R. Micnas, and P. Rożek, Phys. Rev. A **92**, 013602 (2015).
[6] T. P. Polak and T. K. Kopeć, J. Phys. B **42**, 095302 (2009).
[7] K. Jiménez-García, R. L. Compton, Y.-J. Lin, W. D. Phillips, J. V. Porto, and I. B. Spielman, Phys. Rev. Lett. **105**, 110401 (2010).
[8] E. Toth and P. B. Blakie, Phys. Rev. A **83**, 021601 (2011).
[9] F. Gerbier, S. Trotzky, S. Fölling, U. Schnorrberger, J. Thompson, A. Widera, I. Bloch, L. Pollet, M. Troyer, B. Capogrosso-Sansone *et al.*, Phys. Rev. Lett. **101**, 155303 (2008).
[10] A. Hoffmann and A. Pelster, Phys. Rev. A **79**, 053623 (2009).
[11] Q. Zhou and T. L. Ho, Phys. Rev. Lett. **106**, 225301 (2011).
[12] T. Roscilde, Phys. Rev. Lett. **112**, 110403 (2014).
[13] F. Meinert, M. Panfil, M. J. Mark, K. Lauber, J.-S. Caux, and H.-C. Nägerl, Phys. Rev. Lett. **115**, 085301 (2015).
[14] A. Reischl, K. P. Schmidt, and G. S. Uhrig, Phys. Rev. A **72**, 063609 (2005).
[15] H. U. R. Strand, M. Eckstein, and P. Werner, Phys. Rev. A **92**, 063602 (2015).
[16] T. Zaleski and T. Kopeć, Phys. B Condens. Matter **433**, 37 (2014).
[17] M. Endres, T. Fukuhara, D. Pekker, M. Cheneau, P. Schauß, C. Gross, E. Demler, S. Kuhr, and I. Bloch, Nature **487**, 454 (2012).
[18] L. Pollet and N. Prokof'ev, Phys. Rev. Lett. **109**, 010401 (2012).
[19] L. Liu, K. Chen, Y. Deng, M. Endres, L. Pollet, and N. Prokof'ev, Phys. Rev. B **92**, 174521 (2015).
[20] J. Schachenmayer, L. Pollet, M. Troyer, and A. J. Daley, Phys. Rev. A **89**, 011601 (2014).
[21] M. J. Mark, E. Haller, K. Lauber, J. G. Danzl, A. J. Daley, and H.-C. Nägerl, Phys. Rev. Lett. **107**, 175301 (2011).
[22] D. Jaksch, C. Bruder, J. I. Cirac, C. W. Gardiner, and P. Zoller, Phys. Rev. Lett. **81**, 3108 (1998).
[23] M. P. A. Fisher, P. B. Weichman, G. Grinstein, and D. S. Fisher, Phys. Rev. B **40**, 546 (1989).
[24] H. A. Gersch and G. C. Knollman, Phys. Rev. **129**, 959 (1963).
[25] S. Fölling, A. Widera, T. Müller, F. Gerbier, and I. Bloch, Phys. Rev. Lett. **97**, 060403 (2006).
[26] G. K. Campbell, J. Mun, M. Boyd, P. Medley, A. E. Leanhardt, L. G. Marcassa, D. E. Pritchard, and W. Ketterle, Science **313**, 649 (2006).
[27] C. Kollath, A. Iucci, T. Giamarchi, W. Hofstetter, and U. Schollwöck, Phys. Rev. Lett. **97**, 050402 (2006).
[28] J.-W. Huo, F.-C. Zhang, W. Chen, M. Troyer, and U. Schollwöck, Phys. Rev. A **84**, 043608 (2011).
[29] S. R. Clark and D. Jaksch, New J. Phys. **8**, 160 (2006).
[30] M. Łącki, D. Delande, and J. Zakrzewski, Phys. Rev. A **86**, 013602 (2012).
[31] K. zu Münster, F. Gebhard, S. Ejima, and H. Fehske, Phys. Rev. A **89**, 063623 (2014).
[32] S. Ejima, H. Fehske, F. Gebhard, K. zu Münster, M. Knap, E. Arrigoni, and W. von der Linden, Phys. Rev. A **85**, 053644 (2012).
[33] M. Knap, E. Arrigoni, and W. von der Linden, Phys. Rev. B **81**, 235122 (2010).
[34] M. Knap, E. Arrigoni, and W. von der Linden, Phys. Rev. B **81**, 024301 (2010).
[35] P. Pippan, H. G. Evertz, and M. Hohenadler, Phys. Rev. A **80**, 033612 (2009).
[36] K. Sengupta and N. Dupuis, Phys. Rev. A **71**, 033629 (2005).
[37] A. S. Sajna, T. P. Polak, and R. Micnas, Phys. Rev. A **89**, 023631 (2014).
[38] K. Sheshadri, H. R. Krishnamurthy, R. Pandit, and T. V. Ramakrishnan, Europhys. Lett. **22**, 257 (1993).
[39] S. Konabe, T. Nikuni, and M. Nakamura, Phys. Rev. A **73**, 033621 (2006).
[40] Y. Ohashi, M. Kitaura, and H. Matsumoto, Phys. Rev. A **73**, 033617 (2006).
[41] D. B. M. Dickerscheid, D. van Oosten, P. J. H. Denteneer, and H. T. C. Stoof, Phys. Rev. A **68**, 043623 (2003).
[42] Y. Yu and S. T. Chui, Phys. Rev. A **71**, 033608 (2005).
[43] X. Lu, J. Li, and Y. Yu, Phys. Rev. A **73**, 043607 (2006).
[44] D. van Oosten, P. van der Straten, and H. T. C. Stoof, Phys. Rev. A **63**, 053601 (2001).
[45] H. T. C. Stoof, K. B. Gubbels, and D. B. M. Dickerscheid, *Ultracold Quantum Fields* (Springer, Berlin, 2009).
[46] E. Altman and A. Auerbach, Phys. Rev. Lett. **89**, 250404 (2002).
[47] S. D. Huber, E. Altman, H. P. Büchler, and G. Blatter, Phys. Rev. B **75**, 085106 (2007).
[48] J. K. Freericks, H. R. Krishnamurthy, Y. Kato, N. Kawashima, and N. Trivedi, Phys. Rev. A **79**, 053631 (2009).
[49] F. Gerbier, Phys. Rev. Lett. **99**, 120405 (2007).
[50] W. S. Bakr, a. Peng, M. E. Tai, R. Ma, J. Simon, J. I. Gillen, S. Fölling, L. Pollet, and M. Greiner, Science **329**, 547 (2010).
[51] J. Sherson, C. Weitenberg, M. Endres, M. Cheneau, I. Bloch, and S. Kuhr, Nature (London) **467**, 68 (2010).
[52] S. L. Shmakov, Int. J. Pure Appl. Math. **71**, 251 (2011).
[53] M. Ohliger and A. Pelster, World J. Condens. Matter Phys. **03**, 125 (2013).
[54] C. Kollath, A. Iucci, I. P. McCulloch, and T. Giamarchi, Phys. Rev. A **74**, 041604 (2006).
[55] A. Iucci, M. A. Cazalilla, A. F. Ho, and T. Giamarchi, Phys. Rev. A **73**, 041608 (2006).
[56] F. Gerbier, A. Widera, S. Fölling, O. Mandel, T. Gericke, and I. Bloch, Phys. Rev. A **72**, 053606 (2005).
[57] W. Zwerger, J. Opt. B **5**, S9 (2003).
[58] V. A. Kashurnikov, N. V. Prokof'ev, and B. V. Svistunov, Phys. Rev. A **66**, 031601 (2002).
[59] S. Wessel, F. Alet, M. Troyer, and G. G. Batrouni, Phys. Rev. A **70**, 053615 (2004).
[60] Q. Zhou, Y. Kato, N. Kawashima, and N. Trivedi, Phys. Rev. Lett. **103**, 085701 (2009).
[61] A. S. Sajna and T. P. Polak, Phys. Rev. A **90**, 043603 (2014).